ACS NANO

ARTICLE

Multichannel Detection and Differentiation of Explosives with a Quantum Dot Array

William J. Peveler,*[,†,‡] Alberto Roldan,[‡,¶] Nathan Hollingsworth,[‡] Michael J. Porter,[‡] and Ivan P. Parkin*[,‡]
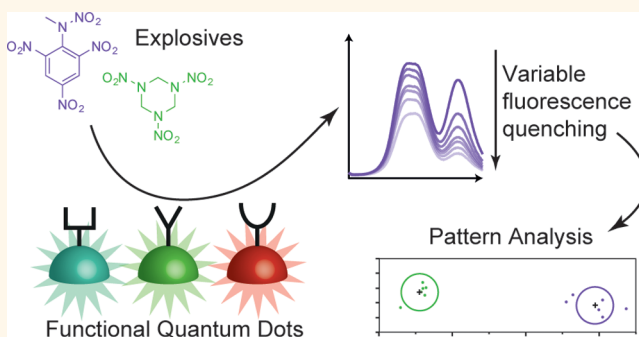
[†]Department of Security and Crime Science, University College London, 35 Tavistock Sq., London WC1H 9EZ, United Kingdom
[‡]Department of Chemistry, University College London, 20 Gordon St., London WC1H 0AJ, United Kingdom
[¶]School of Chemistry, Cardiff University, Main Building, Park Place, Cardiff CF10 3AT, United Kingdom

S *Supporting Information*

ABSTRACT: The sensing and differentiation of explosive molecules is key for both security and environmental monitoring. Single fluorophores are a widely used tool for explosives detection, but a fluorescent array is a more powerful tool for detecting and differentiating such molecules. By combining array elements into a single multichannel platform, faster results can be obtained from smaller amounts of sample. Here, five explosives are detected and differentiated using quantum dots as luminescent probes in a multichannel platform: 2,4-dinitrotoluene (DNT), 2,4,6-trinitrotoluene (TNT), tetryl (2,4,6-trinitrophenylmethylnitramine), cyclotrimethylene-trinitramine (RDX), and pentaerythritol tetranitrate (PETN). The sharp, variable emissions of the quantum dots, from a single excitation wavelength, make them ideal for such a system. Each color quantum dot is functionalized with a different surface receptor via a facile ligation process. These receptors undergo nonspecific interactions with the explosives, inducing variable fluorescence quenching of the quantum dots. Pattern analysis of the fluorescence quenching data allows for explosive detection and identification with limits-of-detection in the ppb range.

KEYWORDS: quantum dot, TNT, sensor, luminescence, explosive, multichannel

D etection of small amounts of explosive material is a key challenge in both the securing of public spaces and vulnerable targets and the environmental monitoring of drinking and waste waters. The application of cross-reactive arrays to chemical sensing is a major advance for the detection of a range of these analytes, without the need for highly specific antibody or similar tests.[1−3] Array-based sensing can differentiate between multiple components within complex mixtures, as well as allowing detection of previously unknown or unexpected analytes without the need for a new sensor. Previous examples have focused on using electrochemical sensors and colorimetric dyes, and advances in computing power allow for application of machine learning techniques to rapidly classify sensing results with a variety of multivariate statistical techniques.[4−8] The use of nanoparticle-based sensors by Rotello *et al.* for biosensing has introduced another powerful tool to array-based chemical sensing, and the new direction of this work focuses on multichannel sensing; combining elements of the cross-reactive array in a single test with multiple outputs, for example, multiple color channels, to reduce the sample volume required and increase sample throughput.[9−11]

Explosive detection is a problem that lends itself well to such an array-based technique. Monitoring of types and levels of explosive in the environment is an active challenge in the security and environmental safety domains,[12,13] with the U.S. Environmental Protection Agency (EPA) setting limits on 2,4-dinitrotoluene (DNT), 2,4,6-trinitrotoluene (TNT), and cyclo-trimethylenetrinitramine (RDX) in drinking water (<0.1 mg/L). Fluorescent nanoparticle-based sensing systems lend themselves to multichannel sensing due to their wide variety of colors and sharp emission peaks.[14] It has been shown that quantum dots (QDs) bind a range of explosives in different ways, bringing the explosive into close proximity with the fluorescent nanoparticles, causing electron-transfer-mediated fluorescence quenching.[15−20] The differential binding between different QD surfaces gives rise to variable fluorescence quenching, allowing a sensing array to be created. Although several simple QD systems have been described for nitro-aromatic explosives, such as TNT and picric acid, particularly

focusing on the formation of Meisenheimer complexes between the electron-poor aromatics and electron-rich amines,[21] few have tried to discriminate between multiple types of explosive.[22−24]

Herein we report a multichannel nanoparticle array for the detection of explosives in a rapid single fluorometric test. It is based on a system of cross-reactive surface functionalities comprised of two macrocyclic (calixarene and cyclodextrin) and two simple (−OH and −OMe) surfaces on multicolored, fluorescent QDs. The system is designed to respond to a range of explosives through supramolecular interactions, such as host−guest binding, electrostatics, and π−π stacking, causing fluorescence quenching of the QDs, to create an analytical fingerprint (Figure 1). It is tested against five explosives, DNT,
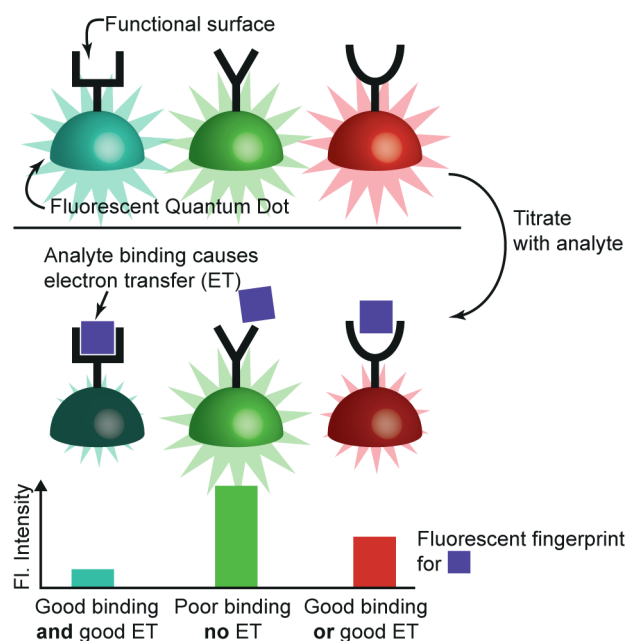

Figure 1. Scheme of sensing mechanism. Differential analyte binding across the multicoloured QD array gives a fluorescent fingerprint for the analyte that can be analyzed computationally.

TNT, tetryl, RDX, and pentaerythritol tetranitrate (PETN) using single channel analysis, demonstrating 100% specificity. The system is created in methanol for compatibility with widely used methanolic solid-phase extraction techniques. Multi-channel explosive sensing is then demonstrated using three of the QD sensors with high sensitivity and specificity.

RESULTS AND DISCUSSION

System Design and Synthesis. Host−guest interactions mediated by macrocyclic hosts are a powerful tool for cross-reactive binding studies.[25] Here, two macrocycles were selected to form cross-reactive QD surfaces: calix[4]arene (**CX**) and β-cyclodextrin (**CD**). Calixarenes have small but open and flexible aromatic cavities (∼3 Å),[26] allowing for π−π interactions with aromatic guests.[27] Cyclodextrins have a larger, more rigid cavity (∼5.7 Å)[28] and are entirely aliphatic, cyclic glucopyranoside oligomers, giving very different receptor characteristics.[25] To supplement these, **OH** and **OMe** surface functionalities were created to give differential reactivity (Figure 2).

Red, green, and blue QDs were synthesized by decomposition of CdO and trioctylphosphine-Se at high temperature by varying reaction times, then shelled with ZnS via

decomposition of Zn-dithiocarbamate onto the surface (Figure S7).[29−31]

The surface bound receptors in this study were designed with a lipoic acid (LA) headgroup, a short triethylene glycol (TEG) spacer for solubility and the surface functionality itself (**CX**, **CD**, **OH**, or **OMe**). A short ethylene glycol was used to ensure close proximity of the bound analyte to the nanoparticle surface, facilitating better electron transfer. An azido-click approach was taken to the ligand synthesis. Azide terminated LA-TEG was produced, and the macrocycles were mono-functionalized with alkynes using literature procedures.[32,33] A click-coupling was performed using copper immobilized on carbon, in the presence of base.[34] This strategy allows for future variation in the library of surface functionalities, potentially enabling attachment of any alkyne functionalized moiety.

The QD ligand exchange was achieved with 365 nm UV-light on the LA moiety in a biphasic hexane/MeOH system.[35,36] This QD functionalization does not require protected thiols or borohydride salts and gives good control over ratios of different receptors on the surface of the nanoparticle. This proved useful for tailoring solubility of the particles. **CX** capped QDs produced with this method were not fully soluble in MeOH so a 3:2 mix of **CX** to **OMe** was used to give full solubility. All other ligand surfaces were fully composed of the named ligand. It has been shown that this procedure can introduce up to 200 ligands per QD, however in this case, it is likely to be fewer due to the larger size of the terminal functionality and shorter chain length.[37]

Initially each surface ligand (**CD**, **CX**, **OH**, and **OMe**) was assembled onto green QDs (em. 544 nm) to create CD_{544}, CX_{544}, OH_{544}, and OMe_{544}. In addition red QDs (em. 608 nm) CX_{608}, OMe_{608} and blue QD (em. 516 nm) OH_{516} were produced and tested. The QDs produced were air stable and stored in the refrigerator without significant loss of fluorescence for 3 months.

Sensing. Methanolic solutions of each QD were titrated with one of five explosives of interest: DNT, TNT, tetryl, RDX, and PETN, in a single channel fashion - one type of QD per test. These explosives were selected on the basis of current threats and to test a range of different analyte functionalities (structures given in Figure 2(ii)). On mixing, the ligand should bind the explosive, and an electron-transfer mechanism between the QD and the electron-deficient explosive causes QD fluorescence quenching. The final concentration of explosive in the solution was varied between 15 and 85 μM with the aim of obtaining a linear quenching regime (approximately 1−30 ppm dependent on explosive mass). Figure 3a illustrates the quenching results of each single channel QD for each analyte. The rate of quenching was measured and found to be <10 s in all cases. An exemplar kinetic curve is given in Figure S12.

Of the green channel QDs, CX_{544} showed good quenching for TNT and tetryl, and to a lesser extent DNT. For example TNT achieved maximal %Quenching $[\%Q = 100 \times (1 - I/I_0)]$ of 73%Q and had a limit of detection (LOD) of <0.1 μg/mL. Tetryl had a maximal 47%Q and a LOD = 1.2 μg/mL (Table S2). The response of the **CX** surface is justified through π-system interactions between the calixarene and the electron-deficient arene systems of TNT, tetryl, and DNT, causing strong binding between analyte and QD, and the relative efficiencies of the ET process between the QD and the analyte. Although PETN was hard to detect, often causing the least quenching of all the analytes, CD_{544} achieved a greater response
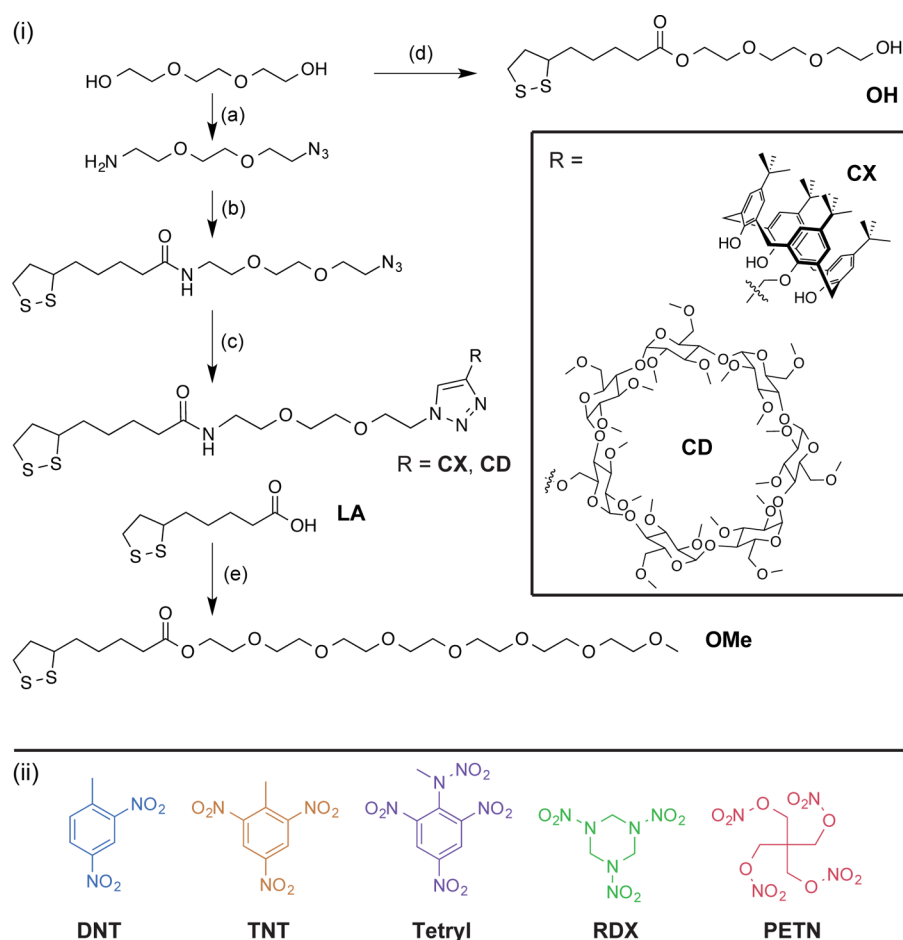
Figure 2. Synthesis and molecules used for surface creation and testing. (i, a) Mesyl chloride, triethylamine (TEA), THF, RT, then NaN$_3$, H$_2$O, 100 °C, then PPh$_3$, 1 M HCl, EtOAc, RT, 65%; (b) LA, DCC, DMAP, DCM, RT, 97%; (c) Cu@C catalyst, monopropargyl cavitand, TEA, dioxane, 70 °C, 3 days; (d) as (b), 0.1 equiv LA, 60%; and (e) methoxyPEG 350, as (b), 82%. (ii) Analytes tested.

to PETN than for DNT. The PETN response from **CD**$_{544}$ is small (16%Q at maximum), implying poor electron transfer between analyte and QD, but the increased response as compared to DNT or RDX gives a good discriminant for this compound. It is possible that the PETN could bind one arm inside the hydrophobic **CD** cavity, due to its greater flexibility compared to the rigid aromatic explosives.[38,39]

QDs **OH**$_{544}$ and **OH**$_{516}$ gave a similar response to the five analytes, likewise **CX**$_{544}$ and **CX**$_{608}$, implying that for the most part, the different color QDs are interchangeable with the different functional surfaces. However, **OMe**$_{608}$ gave far higher quenching responses than its green counterpart, in particular to TNT and tetryl, achieving maxima of 85%Q and 77%Q, respectively. This behavior makes **OMe**$_{608}$ a useful stand-alone sensor for nitro-aromatics with a limit of detection of <0.2 μg/ mL for DNT, TNT, and tetryl, giving rise to the potential for naked-eye detection (Figure 4). Test strips impregnated with **OMe**$_{608}$ could successfully detect TNT and tetryl clearly. Explosives DNT, RDX, and PETN gave some degree of quenching, but particularly with the latter two, there was not enough for naked-eye detection on the strip.

This deviation from the expected response could be due to the larger and less spherical (Figure S7c) red QDs having a lower ligand surface coverage, allowing the more rigid, planar, arene analytes to effectively slip down the gaps between the **OMe** ligands and interact more closely with the QD surface, thus facilitating a stronger quenching. It has been recently

stated that dithiol headgroups, such as dihydrolipoic acid, provide less surface protection than monothiols at low adsorbate concentrations but are less likely to be displaced, thus ensuring longer term colloidal stability.[40] These larger %Q values are not observed for **CX**$_{608}$ due to the bulky ligand headgroup, providing more effective surface sheilding. To explore this, we modeled how the analytes might interact with the QD surface.

***Ab Initio* Modeling.** *Ab initio* methods (described in full in the Supporting Information (SI) Section 4) were applied to probe whether binding of the analytes to the particle surface was feasible and to measure the resulting distortion of the electronic structure. Despite the small size of the CdSe@ZnS QD, they are large enough to be modeled as a periodic slab of ZnS. Thus, a model of wurzite ZnS (110) was developed with density functional methods, as described in the SI.[41] Reduced functional approximations of each of the five analytes were then tested on the surface to measure the extent of the adsorption on the pristine ZnS (110) surface (Figures 5, S8, and S9). The results, summarized in Table 1, show that thiols, as expected, form strong surface bonds, and although the analytes can bind to the surface it is unlikely the thiols are displaced. Nitroaromatics showed little interaction through the aromatic ring but did bind to the surface through the nitro-groups. Increase in the number of nitro groups did not significantly increase the binding potential. Finally nitroaliphatics were
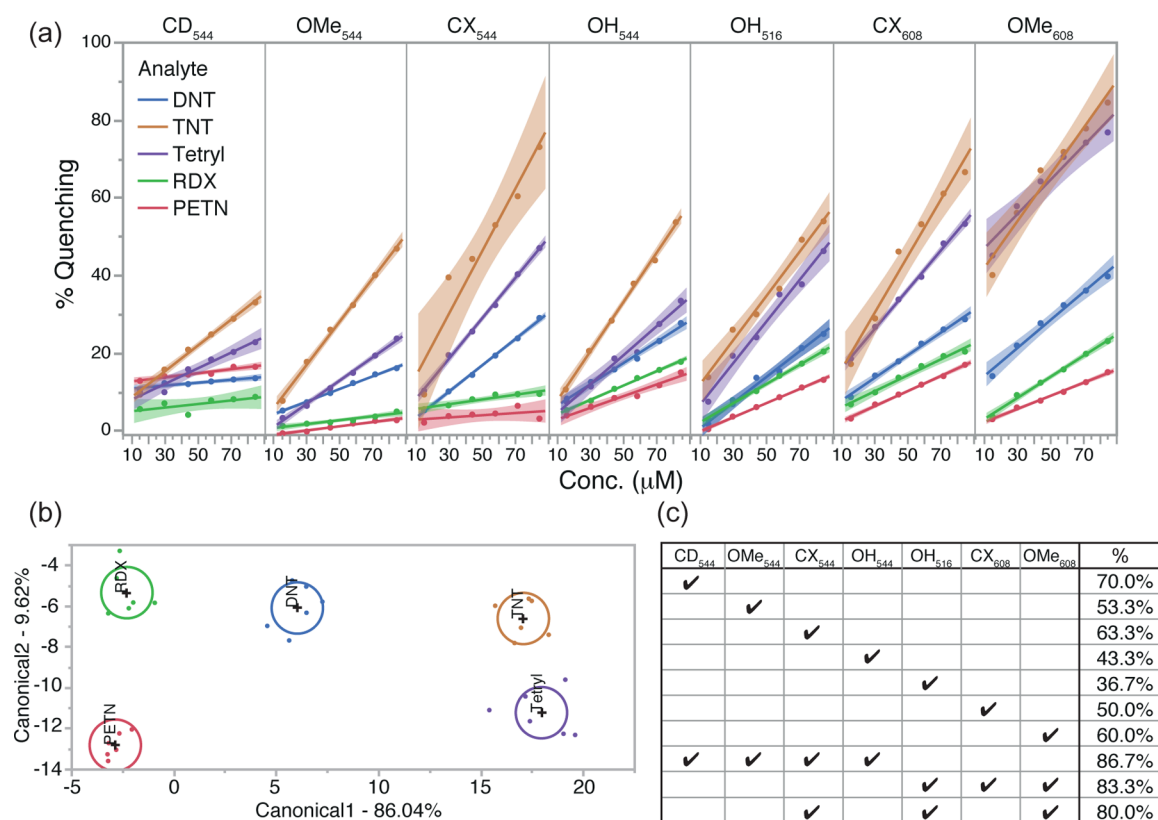
Figure 3. Results of single channel sensing with seven red, green, and blue QDs. (a) %Quenching for each QD for a range of analyte concentrations. Lines indicate best linear fit by least-squares, and shading indicates confidence of fit. (b) Canonical plot (LDA) for %Q data set. Ellipses indicate 95% CI of the mean. Data are classified with 100% accuracy. (c) Jackknifed analysis of same data set showing classification % for several subsets of the array, indicated by ticks, to illucidate the discriminatory power of each QD, indicated by the % of correct classification for that subset.
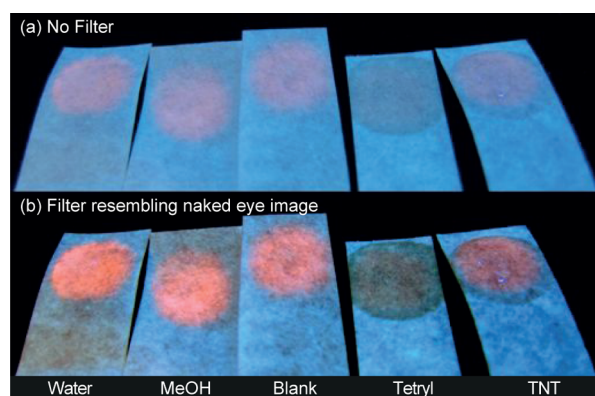

Figure 4. Detection by eye. (a) Five test strips prepared with OMe$_{608}$ on filter paper, exposed to drops of water, MeOH, tetryl, and TNT (detailed in SI). Quenching is observed for tetryl and TNT, although TNT still has some residual brightness in the center. As the camera did not record the brightness of the QDs well under blacklight, postprocessing was performed to improve contrast against background, to simulate what is seen by eye (b).

modeled, and nitrate esters and nitroamines were shown to also bind, however nitroamines bound more favorably.

In the case of **OMe$_{608}$**, if each analyte was reaching the surface, then we would expect nitroaromatics to affect fluorescence substantially due to reasonable binding and electronic structure modification. However, we predict a low response from nitrate esters due to low binding, despite their

good electron withdrawal, and strong binding of nitroamines, but no charge transfer. This model is simplified because it does not account for additional electron-withdrawing groups on the different analytes, for example, TNT vs DNT, nor the sterics between molecules and capping ethylene glycol chains or other lateral interactions. Accounting for the extra NO$_2$ groups on TNT and tetryl and the steric bulk of PETN and RDX, the expected series is tetryl ≃ TNT > DNT > RDX ≃ PETN, which is as observed. This adds weight to the theory of analyte penetration of the ligand surface of **OMe$_{608}$**.

Chemical Nose/Tongue for Explosives Sensing. The differential quenching of each QD by each analyte was used to build up fingerprints for the analytes in the range of concentrations (full details given in Methods). The fluorescence quenching was expressed as either Stern−Volmer quenching (SV = I_0/I) or percentage quenching (%Q). These fingerprints were then analyzed with machine learning techniques to investigate the classification accuracy achieved. The models were blind to the concentration data. Linear discriminant analysis (LDA) was employed, and as a comparator, a support vector machine (SVM) utilizing 10-fold cross validation was tested,[4] but returned poorer classification results (Tables S5 and S6).

We examined first whether SV or %Q data provided better classification power. LDA analysis of the full data set attained 100% classification accuracy in each case, but the −2logLikelihood score for the SV data of 0.389 indicated that it performed slightly worse than analysis of %Q data, with −2logLikelihood = 0.001 (see SI for discussion of negative loglikelihoods, but
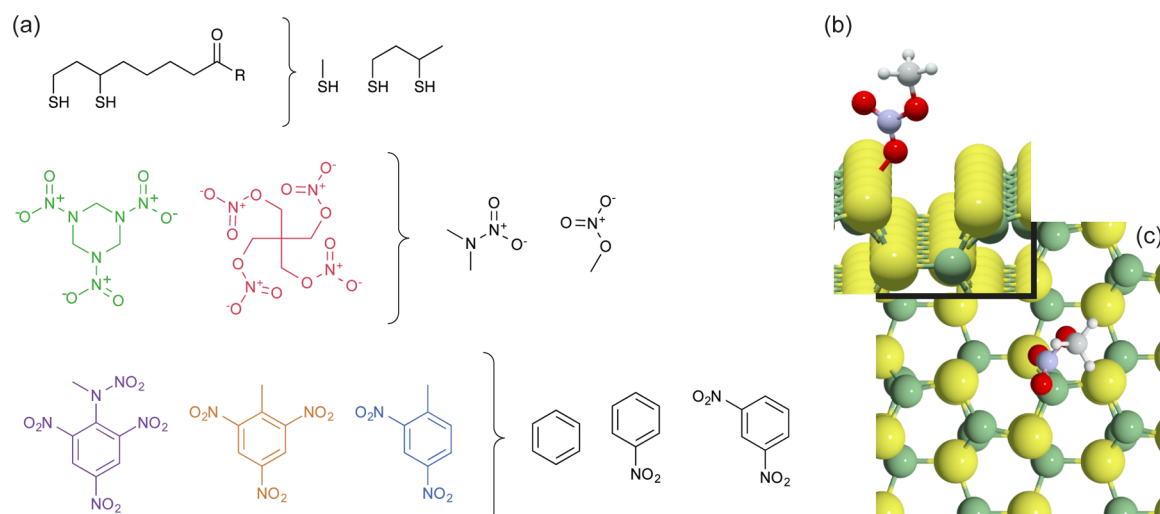
Figure 5. Modeling of surface interactions. (a) First approximations of analytes and surface bound thiol. Example of nitrate ester bound to slab in (b) side on and (c) top down profile.

Table 1. Summary of Adsorption Parameters: Binding Energy Per Site (E_B), Charge Transfer (Δq), Band Gap (E_g), and Work Function (ϕ) Compared with Pristine ZnS(110) Surface

approximation	E_B (eV)	Δq (eV)	E_g (eV)	ϕ (eV)
single thiol	−0.72	−0.1	2.06	3.5
dihydrolipoic acid	−0.50	−0.1	2.05	3.5
benzene	−0.15	0.0	2.06	3.7
nitrophenol	−0.19	0.0	1.32	4.0
dinitrophenol	−0.20	0.2	0.63	4.7
nitrate ester	−0.17	0.8	1.82	3.6
nitroamine	−0.48	−0.2	2.03	3.4

simply put, the smaller the number the better). This difference is further illustrated in the canonical plots for each analysis (also explained further in the SI). The %Q plot ellipses (95% confidence limit of the data mean) are all well separated (Figure 3b), whereas for the SV data (Figure S10) there is close proximity between the TNT and DNT ellipses.

To investigate which QDs had the most discriminatory power in the array, a jackknifed analysis was conducted, using the %Q data set, running the LDA multiple times including only a subset of the particles in turn (Figure 3c). As expected, removing quenching information decreased classification accuracy and indicated that the most powerful discriminating elements were **OMe$_{608}$**, due to its large quenching response to aromatics, and **CD$_{544}$** due to its differential response to PETN.
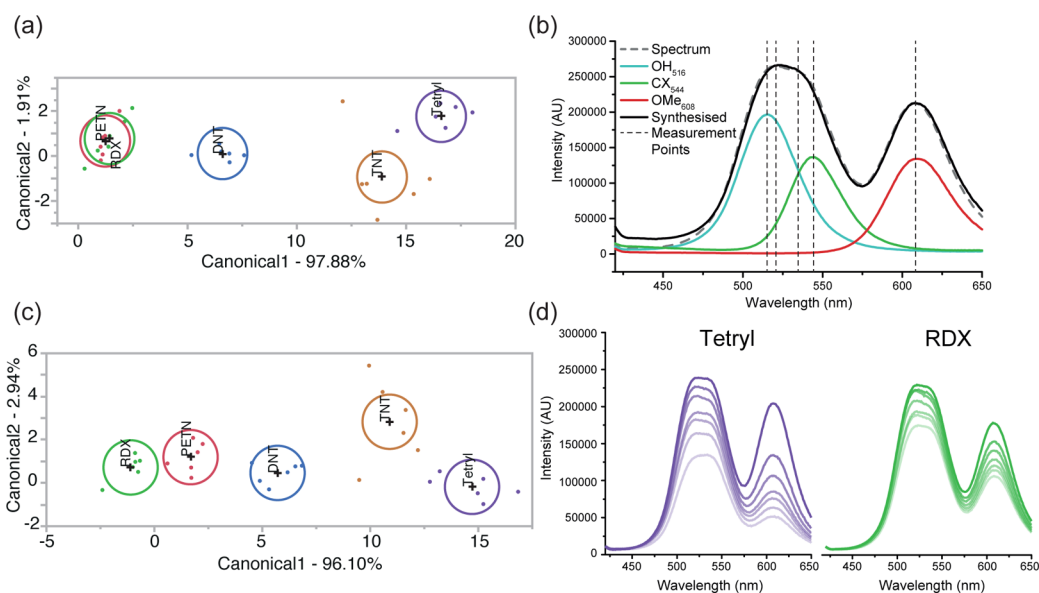

Figure 6. Results of multichannel sensing. (a) Canonical plot for LDA analysis of single channel data approximating the multichannel example with OH$_{516}$, CX$_{544}$, and OMe$_{608}$. Ellipses show 95% CI on the mean. Classification accuracy is 80%. (b) Calculated fit of the three QDs to give composite curve relative to obtained fluorescence spectrum. (c) Canonical plot for multichannel array with %Q data for 516, 520, 533, 544, and 608 nm. Classification accuracy is 100%. (d) Sample titration curves for tetryl and RDX against the multichannel system, with increasing concentration decreasing the fluorescence.

It was also shown that by choosing a subset of the seven QDs, good classification accuracy could still be achieved. A single channel array using the four 544 nm QDs could classify the data with 87% accuracy. Thus, a multichannel (mixed element in a single test) sensor was designed to utilize three different colored QDs, each bearing a different surface functionality. Other considerations were selecting the most discriminating elements and choosing those that gave the largest dynamic response, to provide clear peaks in the more complex spectral environment. OH_{516}, CX_{544}, and OMe_{608} were selected for the reasons above, and when modeled as a subset of the single channel data gave a classification accuracy of 80%, suggesting that a multichannel sensor would be successful (Figure 6a).

To create a multichannel sensor for explosives, the three QDs (OH_{516}, CX_{544}, and OMe_{608}) were mixed. The final spectrum was confirmed by recombination of individual QD spectra to ensure there were no interaction effects between the individual elements (Figure 6b). On excitation at 365 nm, the analytes were titrated at the same concentrations as before, and the principal QD emission wavelengths were monitored, as well as two intermediate wavelengths in the overlap regions between peaks (516, 520, 533, 544, and 608 nm). LOD analysis on the data was hard to perform for RDX and PETN, due to nonlinear responses, but for nitroaromatics tetryl and TNT, LODs of <1 μg/mL and 0.2 μg/mL were obtained respectively, across the whole array (Table S3).

The change in fluorescence at the five points, at different concentrations was then used to train and test LDA and SVM models with SV and %Q data sets as before. LDA analysis on the %Q data set performed better than a simple combination of the three individual channels from the single channel data set, scoring 100% classification accuracy (−2logLikelihood = 1.51) (Figure 6c). The availability of intermediate wavelengths in the multichannel setting allows for this improved classification accuracy, by probing the cross-reactivity between the three sensor elements directly in a single test. The SV data set again performed worse, only scoring 83.3% accuracy (Figure S11).

Jackknifed analysis was performed with the most successful (%Q LDA) model to investigate the classification power of each wavelength (Table S4). It was found that no one wavelength contributed particularly overall to the predictive power of the array, with most individual QD or intermediate emissions scoring giving 40% classification accuracy by themselves. Removing the intermediate wavelengths (520 and 533 nm) leaving the three principal emission peaks in the data set did score 100% classification accuracy, but with −2logLikelihood = 7.98, indicating a greater risk of misclassification. However, the fact that perfect accuracy is achievable with these three wavelengths, in comparison to the 80% achieved by the combination of the three single channel results, highlights the advantages of a multichannel array.

Finally, the effect of contaminants on the array was examined. The methanolic array was dosed with either untreated London tap water (containing trace Cl^-, NO_3^-, Na^+, etc.) or a solution of nitrobenzene. In each case the contaminant addition did not substantially alter the array fluorescence, and on addition of TNT, quenching was still observed of the same magnitude as in ideal conditions (Figure S13). However, it was observed that red OMe_{608} channel was the least stable element to contaminants, with more variation on dilution than with the other channels.

CONCLUSIONS

We have created and demonstrated the first multichannel fluorescent nanoparticle array for explosives detection. The array was constructed from multicolour QDs featuring several novel surface ligands with supramolecular functionality. These were synthesized with a facile methodology, easily extendable to other functionalities. Five nitroaromatics and nitroaliphatics could be reliably detected and discriminated by the array, at part-per-million or lower concentrations. The use of array-based sensing with a multichannel platform has created a single sample test for these materials, with a limit-of-detection of <0.2 μg/mL. The multichannel nature of the test ensures that less sample is required and more accurate and rapid results are obtained. This work is the first step toward devising a monitoring system for explosive residues in waste waters with environmental and security applications. It could, for example, be coupled with solid-phase extraction of waters and soils into methanol for a rapid diagnostic test. This work further highlights the power of differential, multichannel arrays for sensing a wide range of chemicals.

METHODS

CdSe/ZnS QDs, LA-PEG-OMe, LA-TEG-OH and other starting materials prepared by literature methods as described in Supporting Information. LA-TEG-CX and -CD were created by the click conjugation of monopropargyl per-methyl-β-cyclodextrin or mono-propargyl calix[4]arene to LA-TEG-N_3 with Cu on an activated carbon support.[34]

To create the QD-ligand conjugates, a protocol based on Palui et al.[35] was used. Thirty μL of an as-synthesized QD solution was added to 710 μL n-hexane in a glass vial. Methanolic tetramethylammonium hydroxide solution (20 mM, 100 μL) and 250 μL of 100 mM methanolic ligand solution were added to form a biphasic mixture. A stirrer bar was added and the atmosphere changed to nitrogen, before the vial was capped and stirred under 5 × 18 W 365 nm UV-bulbs (Philips TL-D). The progress of the reaction was monitored by observing the fluorescence in the methanolic layer, and once the transfer was complete the QDs were mixed with 1 mL 10:1 ethanol/chloroform and 9 mL hexane, to precipitate, before separation and washing via centrifugation three times (4500 rpm, 5 min). The precipitated QDs were resuspended in 1 mL MeOH and stored at 4 °C for further use.

Dilute solutions of each QD were prepared in MeOH (15 μL/mL) and titrated with fixed amounts of 1 mM DNT, TNT, tetryl, RDX, and PETN, to create solutions at 15.2, 29.8, 44.1, 58.0, 71.4, and 84.5 μM. The fluorescence of each solution was measured multiple times to attain a stable average reading. The intensity of the fluorescence peak (I) was used with the initial sample fluorescence (I_0) to measure the Stern−Volmer quenching ($SV = I_0/I$), and %Q was calculated as [%Q = $100 \times (1 − I/I_0)$].

LDA and SVM analysis were performed on a data set consisting of 1 attribute per QD (e.g., %Q-CX_{544} or SV-516 nm) and the class. The concentration data were removed to blind the computer model. LOD fitting and LDA analysis were performed in the JMP 11 software package. SVMs were performed using WLSVM in WEKA. For the SVM, an RBF kernel was applied, and a grid search was used to optimize the cost and gamma kernel values for each data set, followed by 10-fold cross validation with the optimized values.[42,43] Other analysis and modeling was performed in OriginPro.

ASSOCIATED CONTENT

ⓢ Supporting Information

The Supporting Information is available free of charge on the ACS Publications website at DOI: 10.1021/acsnano.5b06433.

Full experimental procedures and characterization data for all new materials, synthesis of known materials.

Nanoparticle TEM and EDS. Materials modeling details. LOD fitting and additional machine learning discussion (PDF)

AUTHOR INFORMATION

Corresponding Authors
*E-mail: william.peveler.11@ucl.ac.uk.
*E-mail: i.p.parkin@ucl.ac.uk.

Notes
The authors declare no competing financial interest.

REFERENCES

(1) You, C.-C.; Miranda, O. R.; Gider, B.; Ghosh, P. S.; Kim, I.-B.; Erdogan, B.; Krovi, S. A.; Bunz, U. H. F.; Rotello, V. M. Detection and Identification of Proteins using Nanoparticle−Fluorescent Polymer 'Chemical Nose' Sensors. *Nat. Nanotechnol.* **2007**, *2*, 318−323.

(2) De, M.; Rana, S.; Akpinar, H.; Miranda, O. R.; Arvizo, R. R.; Bunz, U. H. F.; Rotello, V. M. Sensing of Proteins in Human Serum using Conjugates of Nanoparticles and Green Fluorescent Protein. *Nat. Chem.* **2009**, *1*, 461−465.

(3) Diehl, K. L.; Anslyn, E. V. Array Sensing using Optical Methods for Detection of Chemical and Biological Hazards. *Chem. Soc. Rev.* **2013**, *42*, 8596−8611.

(4) Peveler, W. J.; Binions, R.; Hailes, S. M. V.; Parkin, I. P. Detection of Explosive Markers using Zeolite Modified Gas Sensors. *J. Mater. Chem. A* **2013**, *1*, 2613−2620.

(5) Evans, G. P.; Buckley, D. J.; Skipper, N. T.; Parkin, I. P. Single-walled Carbon Nanotube Composite Inks for Printed Gas Sensors: Enhanced Detection of NO2, NH3, EtOH and Acetone. *RSC Adv.* **2014**, *4*, 51395−51403.

(6) Askim, J. R.; Mahmoudi, M.; Suslick, K. S. Optical Sensor Arrays for Chemical Sensing: The Optoelectronic Nose. *Chem. Soc. Rev.* **2013**, *42*, 8649−8682.

(7) Ivy, M. A.; Gallagher, L. T.; Ellington, A. D.; Anslyn, E. V. Exploration of Plasticizer and Plastic Explosive Detection and Differentiation with Serum Albumin Cross-Reactive Arrays. *Chem. Sci.* **2012**, *3*, 1773−1779.

(8) Ponnu, A.; Edwards, N. Y.; Anslyn, E. V. Pattern Recognition Based Identification of Nitrated Explosives. *New J. Chem.* **2008**, *32*, 848−855.

(9) Bajaj, A.; Miranda, O. R.; Kim, I. B.; Phillips, R. L.; Jerry, D. J.; Bunz, U. H. F.; Rotello, V. M. Detection and Differentiation of Normal, Cancerous, and Metastatic Cells Using Nanoparticle-Polymer Sensor Arrays. *Proc. Natl. Acad. Sci. U. S. A.* **2009**, *106*, 10912−10916.

(10) Elci, S. G.; Moyano, D. F.; Rana, S.; Tonga, G. Y.; Phillips, R. L.; Bunz, U. H. F.; Rotello, V. M. Recognition of Glycosaminoglycan Chemical Patterns using an Unbiased Sensor Array. *Chem. Sci.* **2013**, *4*, 2076−2080.

(11) Rana, S.; B, L. D.; Mout, R.; Saha, K.; Tonga, G. Y.; S, B. E.; Miranda, O. R.; Rotello, C. M.; Rotello, V. M. A Multichannel Nanosensor for Instantaneous Readout of Cancer Drug Mechanisms. *Nat. Nanotechnol.* **2015**, *10*, 65−69.

(12) Abdul-Karim, N.; Blackman, C. S.; Gill, P. P.; Wingstedt, E. M. M.; Reif, B. A. P. Post-Blast Explosive Residue − A Review of Formation and Dispersion Theories and Experimental Research. *RSC Adv.* **2014**, *4*, 54354−54371.

(13) Jurcic, M.; Peveler, W. J.; Savory, C. N.; Scanlon, D. O.; Kenyon, A. J.; Parkin, I. P. The Vapour Phase Detection of Explosive Markers and Derivatives using Two Fluorescent Metal−Organic Frameworks. *J. Mater. Chem. A* **2015**, *3*, 6351−6359.

(14) Michalet, X.; Pinaud, F. F.; Bentolila, L. A.; Tsay, J. M.; Doose, S.; Li, J. J.; Sundaresan, G.; Wu, A. M.; Gambhir, S. S.; Weiss, S. Quantum Dots for Live Cells, in vivo Imaging, and Diagnostics. *Science* **2005**, *307*, 538−544.

(15) Freeman, R.; Finder, T.; Bahshi, L.; Willner, I. Beta-Cyclodextrin-Modified CdSe/ZnS Quantum Dots for Sensing and Chiroselective Analysis. *Nano Lett.* **2009**, *9*, 2073−2076.

(16) Niu, Q.; Gao, K.; Lin, Z.; Wu, W. Amine-Capped Carbon Dots as a Nanosensor for Sensitive and Selective Detection of Picric Acid in Aqueous Solution via Electrostatic Interaction. *Anal. Methods* **2013**, *5*, 6228−6233.

(17) Pazhanivel, T.; Nataraj, D.; Devarajan, V. P.; Mageshwari, V.; Senthil, K.; Soundararajan, D. Improved Sensing Performance from Methionine Capped CdTe And CdTe/ZnS Quantum Dots for the Detection of Trace Amounts of Explosive Chemicals in Liquid Media. *Anal. Methods* **2013**, *5*, 910−916.

(18) Carrillo-Carrión, C.; Simonet, B. M.; Valcárcel, M. Determination of TNT Explosive Based on its Selectively Interaction with Creatinine-Capped CdSe/ZnS Quantum Dots. *Anal. Chim. Acta* **2013**, *792*, 93−100.

(19) Tian, X.; Chen, L.; Qing, X.; Yu, K.; Wang, X.; Wang, X. Hybrid Cadmium Tellurium Quantum Dots for Rapid Visualization of Trace-Level Nitroaromatic Explosives. *Anal. Lett.* **2014**, *47*, 2035−2047.

(20) Sun, X.; Wang, Y.; Lei, Y. Fluorescence Based Explosive Detection: From Mechanisms to Sensory Materials. *Chem. Soc. Rev.* **2015**, *44*, 8019.

(21) Zhang, K.; Zhou, H.; Mei, Q.; Wang, S.; Guan, G.; Liu, R.; Zhang, J.; Zhang, Z. Instant Visual Detection of Trinitrotoluene Particulates on Various Surfaces by Ratiometric Fluorescence of Dual-Emission Quantum Dots Hybrid. *J. Am. Chem. Soc.* **2011**, *133*, 8424−8427.

(22) Freeman, R.; Finder, T.; Bahshi, L.; Gill, R.; Willner, I. Functionalized CdSe/ZnS QDs for the Detection of Nitroaromatic or RDX Explosives. *Adv. Mater.* **2012**, *24*, 6416−6421.

(23) Freeman, R.; Willner, I. Optical Molecular Sensing with Semiconductor Quantum Dots (Qds). *Chem. Soc. Rev.* **2012**, *41*, 4067−4085.

(24) Enkin, N.; Sharon, E.; Golub, E.; Willner, I. Ag Nanocluster/DNA Hybrids: Functional Modules for the Detection of Nitroaromatic and RDX Explosives. *Nano Lett.* **2014**, *14*, 4918−4922.

(25) Ponnu, A.; Anslyn, E. V. A Fluorescence-Based Cyclodextrin Sensor to Detect Nitroaromatic Explosives. *Supramol. Chem.* **2010**, *22*, 65−71.

(26) Gutsche, C. D. In *Calixarenes*; Stoddart, J. F., Ed.; Royal Society of Chemistry: Cambridge, U.K., 1989.

(27) Montmeat, P.; Veignal, F.; Methivier, C.; Pradier, C. M.; Hairault, L. Study of Calixarenes Thin Films as Chemical Sensors for the Detection of Explosives. *Appl. Surf. Sci.* **2014**, *292*, 137−141.

(28) Del Valle, E. M. M. Cyclodextrins and Their Uses: A Review. *Process Biochem.* **2004**, *39*, 1033−1046.

(29) Dethlefsen, J. R.; Døssing, A. Preparation of a ZnS Shell on CdSe Quantum Dots Using a Single-Molecular ZnS Precursor. *Nano Lett.* **2011**, *11*, 1964−1969.

(30) Bear, J. C.; Hollingsworth, N.; McNaughter, P. D.; Mayes, A. G.; Ward, M. B.; Nann, T.; Hogarth, G.; Parkin, I. P. Copper-Doped CdSe/ZnS Quantum Dots: Controllable Photoactivated Copper(I) Cation Storage and Release Vectors for Catalysis. *Angew. Chem., Int. Ed.* **2014**, *53*, 1598−1601.

(31) Bear, J. C.; Hollingsworth, N.; Roffey, A.; McNaughter, P. D.; Mayes, A. G.; Macdonald, T. J.; Nann, T.; Ng, W. H.; Kenyon, A. J.; Hogarth, G.; et al. Doping Group IIB Metal Ions into Quantum Dot

Shells *via* the One-Pot Decomposition of Metal-Dithiocarbamates. *Adv. Opt. Mater.* **2015**, *3*, 704−712.

(32) Chetcuti, M. J.; Devoille, A. M. J.; Othman, A. B.; Souane, R.; Thuéry, P.; Vicens, J. Synthesis of Mono-, Di- and Tetra-Alkyne Functionalized Calix[4]arenes: Reactions of these Multipodal Ligands with Dicobalt Octacarbonyl to give Complexes which Contain up to Eight Cobalt Atoms. *Dalton Trans.* **2009**, 2999−3008.

(33) Faiz, J. A.; Spencer, N.; Pikramenou, Z. Acetylenic Cyclodextrins for Multireceptor Architectures: Cups with Sticky Ends for the Formation of Extension Wires and Junctions. *Org. Biomol. Chem.* **2005**, *3*, 4239−4245.

(34) Lipshutz, B. H.; Taft, B. R. Heterogeneous Copper-in-Charcoal-Catalyzed Click Chemistry. *Angew. Chem., Int. Ed.* **2006**, *45*, 8235−8238.

(35) Palui, G.; Avellini, T.; Zhan, N.; Pan, F.; Gray, D.; Alabugin, I.; Mattoussi, H. Photoinduced Phase Transfer of Luminescent Quantum Dots to Polar and Aqueous Media. *J. Am. Chem. Soc.* **2012**, *134*, 16370−16378.

(36) Zhan, N.; Palui, G.; Grise, H.; Tang, H.; Alabugin, I.; Mattoussi, H. Combining Ligand Design with Photoligation to Provide Compact, Colloidally Stable, and Easy to Conjugate Quantum Dots. *ACS Appl. Mater. Interfaces* **2013**, *5*, 2861−2869.

(37) Zhan, N.; Palui, G.; Merkl, J.-P.; Mattoussi, H. Quantifying the Density of Surface Capping Ligands on Semiconductor Quantum Dots. *Proc. SPIE* **2015**, 93381A−93381A-11.

(38) Cahill, S.; Bulusu, S. Molecular Complexes of Explosives with Cyclodextrins I. Characterization of Complexes with the Nitramines RDX, HMX and TNAZ in Solution by 1H NMR Spin-Lattice Relaxation Time Measurements. *Magn. Reson. Chem.* **1993**, *31*, 731−735.

(39) Zhang, M.; Shi, Z.; Bai, Y.; Gao, Y.; Hu, R.; Zhao, F. Using Molecular Recognition of β-Cyclodextrin to Determine Molecular Weights of Low-Molecular-Weight Explosives by MALDI-TOF Mass Spectrometry. *J. Am. Soc. Mass Spectrom.* **2006**, *17*, 189−193.

(40) Takeuchi, H.; Omogo, B.; Heyes, C. D. Are Bidentate Ligands Really Better than Monodentate Ligands For Nanoparticles? *Nano Lett.* **2013**, *13*, 4746−4752.

(41) Afzaal, M.; Malik, M. A.; O'Brien, P. Preparation of Zinc Containing Materials. *New J. Chem.* **2007**, *31*, 2029−2040.

(42) Chang, C.-C.; Lin, C.-J. LIBSVM: A Library for Support Vector Machines. *ACM Trans. Intell. Syst. Technol.* **2011**, *2*, 1−27.

(43) El-Manzalawy, Y.; Honavar, V. *WLSVM: Integrating LIBSVM into WEKA Environment*, 2005. Software available at http://www.cs.iastate.edu/yasser/wlsvm.